Estimating Neural Sources from Each Time-Frequency Component of Magnetoencephalographic Data

Kensuke Sekihara*, *Member, IEEE*, Srikantan S. Nagarajan, David Poeppel, Satoru Miyauchi, Norio Fujimaki, Hideaki Koizumi, and Yasushi Miyashita

***Abstract*—We have developed a method that incorporates the time-frequency characteristics of neural sources into magnetoencephalographic (MEG) source estimation. This method, referred to as the time-frequency multiple-signal-classification algorithm, allows the locations of neural sources to be estimated from any time-frequency region of interest. In this paper, we formulate the method based on the most general form of the quadratic time-frequency representations. We then apply it to two kinds of nonstationary MEG data: gamma-band (frequency range between 30–100 Hz) auditory activity data and spontaneous MEG data. Our method successfully detected the gamma-band source slightly medial to the N1m source location. The method was able to selectively localize sources for alpha-rhythm bursts at different locations. It also detected the mu-rhythm source from the alpha-rhythm-dominant MEG data that was measured with the subject's eyes closed. The results of these applications validate the effectiveness of the time-frequency MUSIC algorithm for selectively localizing sources having different time-frequency signatures.**

***Index Terms*—Biomagnetism, biomedical signal processing, functional brain imaging, inverse problems, time-frequency analysis.**

I. Introduction

THE NONINVASIVE measurement of magnetic fields generated from human cortical neural activities, referred to as magnetoencephalography (MEG) [1], has been found to be a powerful tool in studies of human neurophysiology and neural information processing. One major problem with MEG measurements is the inverse problem [1], a problem of estimating neural current distributions from the magnetic field measured outside a human head. Because this estimation problem is inherently ill-posed, the estimation needs to incorporate some prior knowledge regarding the source characteristics. Such characteristics can include possible source locations, the source spatial extent, the total number of sources, or the frequency characteristics of source activities.

Neuronal activities in a human brain are basically nonstationary. Time-frequency analysis has, therefore, played an important role in analyzing and characterizing electrophysiological data such as that from MEG or encephalography (EEG) [2]–[4]. We have developed a method that incorporates the time-frequency characteristics of the source activity into the source estimation. The method, referred to as the time-frequency multiple-signal classification (MUSIC) algorithm, allows us to estimate the locations of neural sources from any time-frequency region of interest (ROI). We have reported, in a short communication, the formulation of a method based on the Cohen-class quadratic time-frequency representations [5]. The present paper presents a formulation based on the most general form of the quadratic time-frequency representations. It also presents the results of applying the developed method to two types of nonstationary MEG data: stimulus-locked auditory gamma-band data and spontaneous MEG (alpha and mu rhythm) data.

A recent study investigated the possibility of incorporating source estimation with time-frequency analysis in the form of a two step procedure [6]. They first synthesize a signal that only contains the target time-frequency components of interest, and then apply a single-dipole localization procedure to this synthesized signal. This method relies on a technique referred to as time-frequency synthesis. This technique, however, is tedious and may be computationally intensive when an ROI with an arbitrary shape is used. In contrast, our method, which estimates neural sources directly from the time-frequency domain data, is more straightforward. Note that a method similar to our method was independently developed and reported recently in the radar-signal processing field [7].

The purpose of this paper is to describe the formulation of the time-frequency MUSIC algorithm, and to present the details of our investigation that validate this formulation. Following the method's formulation, which is based on general quadratic time-frequency representations, we present the results from numerical experiments that not only validated the method's formulation, but also showed the basic superiority of the method over existing source-localization methods. We

Manuscript received December 10, 1998; revised November 29, 1999. This work was carried out as part of the MIT-JST International Cooperative Research Project "Mind Articulation." *Asterisk indicates corresponding author*.

*K. Sekihara is with the Mind Articulation Project, Japan Science and Technology Corporation (JST) Yushima 4-9-2, Bunkyo-ku, Tokyo, 113-0034, Japan (e-mail: sekihara@ma.jst.go.jp).

S. S. Nagarajan is with the Keck Center for Integrative Neuroscience, University of California, San Francisco, CA 94143-0732 USA. He is also with the Scientific Learning Corporation, Berkeley, CA 94704 USA.

D. Poeppel is with the Department of Linguistics and Biology, University of Maryland, College Park, MD 20742 USA.

S. Miyauchi and N. Fujimaki are with the Kansai Advanced Research Center, Communications Research Laboratory, Hyogo, 651-2401, Japan.

H. Koizumi is with the Mind Articulation Project, Japan Science and Technology Corporation (JST) Bunkyo-ku, Tokyo, 113-0034, Japan.

Y. Miyashita is with the Mind Articulation Project, Japan Science and Technology Corporation (JST) Bunkyo-ku, Tokyo, 113-0034, Japan. He is also with the Department of Physiology, The University of Tokyo, School of Medicine, Bunkyo-ku, Tokyo, 113-0033, Japan.

Publisher Item Identifier S 0018-9294(00)03282-1.

then apply the time-frequency MUSIC algorithm to auditory gamma-band evoked-field data and spontaneous MEG (alpha and mu rhythm) data. These data were used because the their origins have been relatively well investigated, and we can assess the validity of the time-frequency MUSIC results by comparing them with results from previous investigations [8]–[12]. The results of these applications validated the basic effectiveness of the time-frequency MUSIC algorithm when analyzing such nonstationary MEG signals as mixtures of various time-frequency components.

Throughout this paper, a lower-case boldface font indicates a vector, and an upper-case boldface font indicates a matrix. The superscript T indicates the matrix transpose and the superscript H indicates the Hermitian conjugate transpose of a matrix.

II. Method

A. Definitions

Let us define the magnetic field measured by the mth detector coil at time t as $b_m(t)$ and a vector $\boldsymbol{b}(t) = [b_1(t), b_2(t), \ldots, b_M(t)]^T$ as a set of measured data where M is the total number of detector coils. A total of P current-dipole sources are assumed to generate the biomagnetic field, and the locations of these sources are denoted as $(\boldsymbol{x}_1, \boldsymbol{x}_2, \ldots, \boldsymbol{x}_P)$. The magnitude of the pth dipole-source moment is defined as $s_p(t)$. The source magnitude vector is defined as $\boldsymbol{s}(t) = [s_1(t), s_2(t), \ldots, s_P(t)]^T$. The spherical homogeneous conductor model [13] is used, so we consider two tangential components, the ϕ and θ components, of the source moment while its radial component is assumed to be zero. The dipole orientation is defined as its normal vector $\boldsymbol{\eta}_p(t) = [\eta_p^{\phi}(t), \eta_p^{\theta}(t)]^T$, where $\|\boldsymbol{\eta}_p(t)\| = 1$. We also define a $2P \times P$ matrix that expresses the orientations of all P dipole sources as $\boldsymbol{\Psi}(t)$ such that

$$\boldsymbol{\Psi}(t) = \begin{bmatrix} \boldsymbol{\eta}_1(t) & 0 & \ldots & 0 \\ 0 & \boldsymbol{\eta}_2(t) & \cdot & \vdots \\ \vdots & \cdot & \ddots & 0 \\ 0 & \ldots & 0 & \boldsymbol{\eta}_P(t) \end{bmatrix}. \tag{1}$$

In this paper, for simplicity, we assume that no dipole sources change their orientation during the time period of interest, and we use time-independent $\boldsymbol{\Psi}$ to express the dipole-source orientations.

The lead-field vectors for the ϕ and θ components of the source moment at $\boldsymbol{x}$ are defined as $\boldsymbol{l}^{\phi}(\boldsymbol{x}) = [l_1^{\phi}(\boldsymbol{x}), l_2^{\phi}(\boldsymbol{x}), \ldots, l_M^{\phi}(\boldsymbol{x})]^T$ and $\boldsymbol{l}^{\theta}(\boldsymbol{x}) = [l_1^{\theta}(\boldsymbol{x}), l_2^{\theta}(\boldsymbol{x}), \ldots, l_M^{\theta}(\boldsymbol{x})]^T$. Here, $l_m^{\phi}(\boldsymbol{x})$ and $l_m^{\theta}(\boldsymbol{x})$ express the mth sensor output induced by the unit-magnitude source directed in the ϕ and θ directions, respectively. We define the lead-field matrix for the source at $\boldsymbol{x}$ as $\boldsymbol{L}(\boldsymbol{x}) = [\boldsymbol{l}^{\phi}(\boldsymbol{x}), \boldsymbol{l}^{\theta}(\boldsymbol{x})]$, which represents the sensitivity of the sensor array at location $\boldsymbol{x}$. The composite lead-field matrix for the entire set of P dipole sources is defined as $\boldsymbol{L}_c = [\boldsymbol{L}(\boldsymbol{x}_1), \boldsymbol{L}(\boldsymbol{x}_2), \ldots, \boldsymbol{L}(\boldsymbol{x}_P)]$. Then, the relationship between $\boldsymbol{b}(t)$ and $\boldsymbol{s}(t)$ is expressed as

$$\boldsymbol{b}(t) = [\boldsymbol{L}_c\boldsymbol{\Psi}]\boldsymbol{s}(t) + \boldsymbol{n}(t) \tag{2}$$

where $\boldsymbol{n}(t)$ is the additive noise.

B. Conventional Time-Domain MUSIC Algorithm

The MEG inverse problem is the problem of estimating the source locations $\boldsymbol{x}_1, \ldots, \boldsymbol{x}_P$ and the source activity $\boldsymbol{s}(t)$ from the measurement $\boldsymbol{b}(t)$. The conventional way to solve this inverse problem is to minimize the least-squares error $E = \|\boldsymbol{b}(t) - \hat{\boldsymbol{b}}(t)\|$ where $\hat{\boldsymbol{b}}(t)$ is the estimated measurement. Estimating the source locations, in this minimization, requires a $3P$ dimensional nonlinear search. Generally, for such a highly multidimensional search, there is no guarantee of obtaining a correct solution unless we can set the initial estimate very close to the true solution. The MUSIC algorithm approach has been introduced [14], [15] in order to avoid this highly multidimensional search. A distinct advantage of this algorithm is that regardless of the number of dipole sources, it gives a suboptimal estimate of the source locations by using only a three-dimensional search in the solution space.

We define the measured-data covariance matrix as $\boldsymbol{R}_b$, and the covariance matrix of the dipole-source activities as $\boldsymbol{R}_s$. Using (2) and assuming that the noise and signal are uncorrelated, we have

$$\begin{aligned} \boldsymbol{R}_b &= \langle \boldsymbol{b}(t)\boldsymbol{b}^T(t) \rangle \\ &= (\boldsymbol{L}_c\boldsymbol{\Psi}) \langle \boldsymbol{s}(t)\boldsymbol{s}^T(t) \rangle \left(\boldsymbol{\Psi}^T\boldsymbol{L}_c^T\right) + \langle \boldsymbol{n}(t)\boldsymbol{n}^T(t) \rangle \\ &= (\boldsymbol{L}_c\boldsymbol{\Psi})\boldsymbol{R}_s \left(\boldsymbol{\Psi}^T\boldsymbol{L}_c^T\right) + \sigma^2\boldsymbol{I} \end{aligned} \tag{3}$$

where $\langle \cdot \rangle$ indicates the ensemble average, and it is assumed that the noise is white Gaussian noise with variance σ^2. This equation shows the relationship between the covariance matrices of measurement and source activities; this relationship is the basis of deriving the MUSIC algorithm. We denote the eigenvectors of $\boldsymbol{R}_b$ as $\{\boldsymbol{e}_j\}$, where $j = 1, 2, \ldots, M$ (the eigenvalues are numbered in decreasing order), and define matrix $\boldsymbol{E}_N$ as $\boldsymbol{E}_N = [\boldsymbol{e}_{P+1}, \ldots, \boldsymbol{e}_M]$. The eigenvectors $\{\boldsymbol{e}_{P+1}, \ldots, \boldsymbol{e}_M\}$ are those corresponding to the noise-level eigenvalues, and the span of the columns in the matrix $\boldsymbol{E}_N$ is called the noise subspace.

To estimate the locations of the sources, the MUSIC algorithm takes advantage of the fact that the sensor lead-field with an optimum orientation $\boldsymbol{L}(\boldsymbol{x})\boldsymbol{\eta}_{\mathrm{opt}}$, in which $\boldsymbol{\eta}_{\mathrm{opt}}$ represents the normal vector in the optimum orientation, is orthogonal to the noise subspace of $\boldsymbol{R}_b$ at the true source locations. This orthogonality can be evaluated by the following function [15], which is called the MUSIC localizer

$$J(\boldsymbol{x}) = 1/\lambda_{\min}\left[\boldsymbol{L}^T(\boldsymbol{x})\boldsymbol{E}_N\boldsymbol{E}_N^T\boldsymbol{L}(\boldsymbol{x}),\, \boldsymbol{L}^T(\boldsymbol{x})\boldsymbol{L}(\boldsymbol{x})\right] \tag{4}$$

where $\lambda_{\min}[\cdot, \cdot]$ indicates the generalized minimum eigenvalue of the matrix pair given in parenthesis. Equation (4) is calculated in a volume where sources can exist, and each location where $J(\boldsymbol{x})$ reaches a peak is chosen as the location of one source.

C. Time-Frequency Domain MUSIC Algorithm

1) Covariance-Matrix Relationship in the Time-Frequency Domain: Here, we describe the time-frequency domain MUSIC algorithm, which makes it possible to estimate neural sources from each time-frequency component of MEG data. Time-frequency signal representations are generally classified

into two groups: linear and quadratic representations [16]. Although the linear representations include the well-known short-time Fourier transform (STFT) and the wavelet transform, quadratic time-frequency representations are known to provide better performance, and thus many modern time-frequency representations have quadratic forms [17]. We thus use a general quadratic time-frequency representation to formulate the method, but it can also be easily formulated using linear time-frequency representations.

Let us denote the time-frequency representation matrix of the vector signal $\boldsymbol{b}(t)$ as $\boldsymbol{C}_b(t,\, f)$ and that of $\boldsymbol{s}(t)$ as $\boldsymbol{C}_s(t,\, f)$. In the most general quadratic form, they are expressed as

$$\boldsymbol{C}_b(t,\, f) = \iint_{-\infty}^{\infty} \Phi(t,\, f,\, \nu,\, \xi) \int_{-\infty}^{\infty} \boldsymbol{b}(\nu + \tau/2) \cdot \boldsymbol{b}^T(\nu - \tau/2) e^{-2\pi i \xi \tau}\, d\tau\, d\nu\, d\xi \tag{5}$$

and

$$\boldsymbol{C}_s(t,\, f) = \iint_{-\infty}^{\infty} \Phi(t,\, f,\, \nu,\, \xi) \int_{-\infty}^{\infty} \boldsymbol{s}(\nu + \tau/2) \cdot \boldsymbol{s}^T(\nu - \tau/2) e^{-2\pi i \xi \tau}\, d\tau\, d\nu\, d\xi. \tag{6}$$

The matrix $\boldsymbol{C}_b(t,\, f)$ is an $M \times M$ matrix. Its diagonal elements are the auto-time-frequency distributions of the channel recordings and its off-diagonal elements are the cross-time-frequency distributions between different channel recordings. The matrix $\boldsymbol{C}_s(t,\, f)$ is a $P \times P$ matrix. Its diagonal elements are the auto-time-frequency distributions of the source activities and its off-diagonal elements are the cross-time-frequency distributions between different source activities.

In (5) and (6), $\Phi(t,\, f,\, \nu,\, \xi)$ is a kernel, which determines the characteristics of the resultant quadratic time-frequency distributions [17]. When this kernel has the form $\Phi(t,\, f,\, \nu,\, \xi) = \varphi(\nu - t,\, \xi - f)$, the resultant time-frequency representations are called the Cohen class. When the kernel has a form of the affine smoothing, i.e., $\Phi(t,\, f,\, \nu,\, \xi) = \varphi'((f/f_0)(\nu - t),\, (f_0/f)\xi)$, where f_0 is a constant that converts scale to frequency, the quadratic time-frequency representations are called the affine class. The relationship between several specific choices of the kernel and the properties of the resultant time-frequency distributions has been well studied in the field of time-frequency analysis. A detailed discussions on such studies are found in [16]–[18].

Using (2), (5), and (6), we can derive

$$\boldsymbol{C}_b(t,\, f) = (\boldsymbol{L}_c\boldsymbol{\Psi})\boldsymbol{C}_s(t,\, f)\left(\boldsymbol{\Psi}^T\boldsymbol{L}_c^T\right) + \boldsymbol{C}_{sn}(t,\, f) + \boldsymbol{C}_{ns}(t,\, f) + \boldsymbol{C}_n(t,\, f) \tag{7}$$

where

$$\boldsymbol{C}_{sn}(t,\, f) = \iint_{-\infty}^{\infty} \Phi(t,\, f,\, \nu,\, \xi) \int_{-\infty}^{\infty} (\boldsymbol{L}_c\boldsymbol{\Psi})\boldsymbol{s}(\nu + \tau/2) \cdot \boldsymbol{n}^T(\nu - \tau/2) e^{-2\pi i \xi \tau}\, d\tau\, d\nu\, d\xi \tag{8}$$

$$\boldsymbol{C}_{ns}(t,\, f) = \iint_{-\infty}^{\infty} \Phi(t,\, f,\, \nu,\, \xi) \int_{-\infty}^{\infty} \boldsymbol{n}(\nu + \tau/2) \cdot \boldsymbol{s}^T(\nu - \tau/2)\left(\boldsymbol{\Psi}^T\boldsymbol{L}_c^T\right) e^{-2\pi i \xi \tau}\, d\tau\, d\nu\, d\xi \tag{9}$$

and

$$\boldsymbol{C}_n(t,\, f) = \iint_{-\infty}^{\infty} \Phi(t,\, f,\, \nu,\, \xi) \int_{-\infty}^{\infty} \boldsymbol{n}(\nu + \tau/2) \cdot \boldsymbol{n}^T(\nu - \tau/2) e^{-2\pi i \xi \tau}\, d\tau\, d\nu\, d\xi. \tag{10}$$

Let us introduce the target time-frequency region Ω which contains the signal of interest whose source configuration is to be investigated. We assume that the noise and signal are uncorrelated in the target region, and that the noise is white Gaussian and is uncorrelated between channels. Then, we obtain $\langle \boldsymbol{C}_{ns}(t,\, f)\rangle = \langle \boldsymbol{C}_{sn}(t,\, f)\rangle = 0$ and $\langle \boldsymbol{C}_n(t,\, f)\rangle = \sigma_D^2\boldsymbol{I}$ where $\langle\cdot\rangle$ again indicates the ensemble average and σ_D^2 is the noise-power density in the time-frequency domain. We also assume that the noise has the ergodic property, so the ensemble average can be approximated with the average over the target region, i.e.,

$$\frac{1}{\Omega}\iint_{\Omega} \boldsymbol{C}_{ns}(t,\, f)\, dt\, df \approx \langle \boldsymbol{C}_{ns}(t,\, f)\rangle = 0,$$
$$\frac{1}{\Omega}\iint_{\Omega} \boldsymbol{C}_{sn}(t,\, f)\, dt\, df \approx \langle \boldsymbol{C}_{sn}(t,\, f)\rangle = 0$$

and

$$\frac{1}{\Omega}\iint_{\Omega} \boldsymbol{C}_n(t,\, f) \approx \langle \boldsymbol{C}_n(t,\, f)\rangle = \sigma_D^2\boldsymbol{I}.$$

We also define the matrices $\boldsymbol{\Upsilon}_b$ and $\boldsymbol{\Upsilon}_s$ obtained by averaging $\boldsymbol{C}_b(t,\, f)$ and $\boldsymbol{C}_s(t,\, f)$ over the target time-frequency region

$$\boldsymbol{\Upsilon}_b = \frac{1}{\Omega}\iint_{\Omega} \boldsymbol{C}_b(t,\, f)\, dt\, df$$

and

$$\boldsymbol{\Upsilon}_s = \frac{1}{\Omega}\iint_{\Omega} \boldsymbol{C}_s(t,\, f)\, dt\, df. \tag{11}$$

Then, we finally derive the relationship

$$\boldsymbol{\Upsilon}_b = (\boldsymbol{L}_c\boldsymbol{\Psi})\boldsymbol{\Upsilon}_s(\boldsymbol{\Psi}^T\boldsymbol{L}_c^T) + \sigma_D^2\boldsymbol{I}. \tag{12}$$

This equation shows the relationship between the measurement and source-activity covariance matrices in the time-frequency domain [its conventional time-domain counterpart is shown in (3)], and is the basis of deriving the time-frequency MUSIC algorithm.

2) Deriving the Time-Frequency MUSIC Localizer: We denote the noise-level eigenvectors of $\boldsymbol{\Upsilon}_b$ as $\boldsymbol{u}_j$ $(j = P_\Omega + 1,\, \ldots,\, M)$, where P_Ω is the number of sources whose activity has time-frequency components in the target region. Then, since the noise-level eigenvectors satisfy the relationship, $\boldsymbol{\Upsilon}_b\boldsymbol{u}_j = \sigma_D^2\boldsymbol{u}_j$, (12) leads to

$$\left(\boldsymbol{\Upsilon}_b - \sigma_D^2\boldsymbol{I}\right)\boldsymbol{u}_j = (\boldsymbol{L}_c\boldsymbol{\Psi})\boldsymbol{\Upsilon}_s\left(\boldsymbol{\Psi}^T\boldsymbol{L}_c^T\right)\boldsymbol{u}_j = 0 \qquad j = P_\Omega + 1,\, \ldots,\, M. \tag{13}$$

The matrices $\boldsymbol{L}_c$ and $\boldsymbol{\Psi}$ are full-column-rank matrices. Therefore, when the matrix $\boldsymbol{\Upsilon}_s$ is a full-rank matrix, we get

$$\boldsymbol{\Psi}^T\boldsymbol{L}_c^T\boldsymbol{u}_j = 0 \quad \text{for} \quad j = P_\Omega + 1,\, \ldots,\, M. \tag{14}$$

The above equation indicates that source locations can be obtained by checking the orthogonality between the optimally-ori-

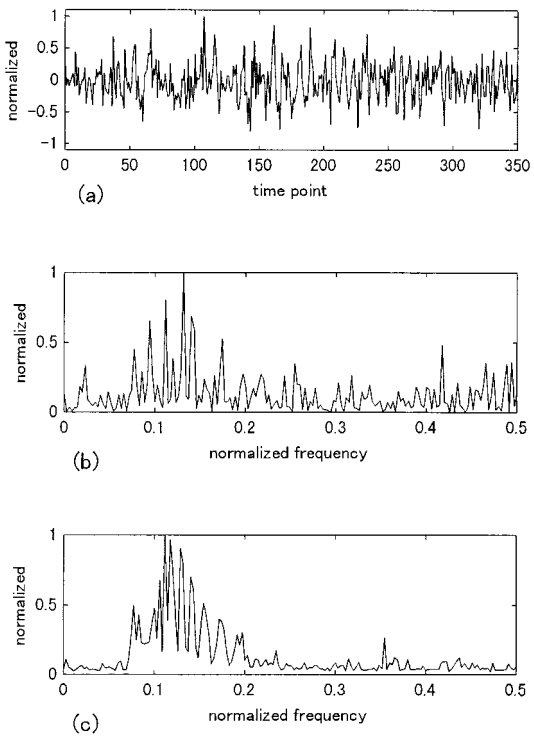

Fig. 1. (a) Waveform of the generated magnetic field from one representative channel located approximately above the sources. (b) Power spectrum of the waveform shown in (a). (c) Power spectrum of the generated magnetic field obtained by averaging the spectra from all channels. The frequency is normalized such that the Nyquist frequency is equal to 0.5.

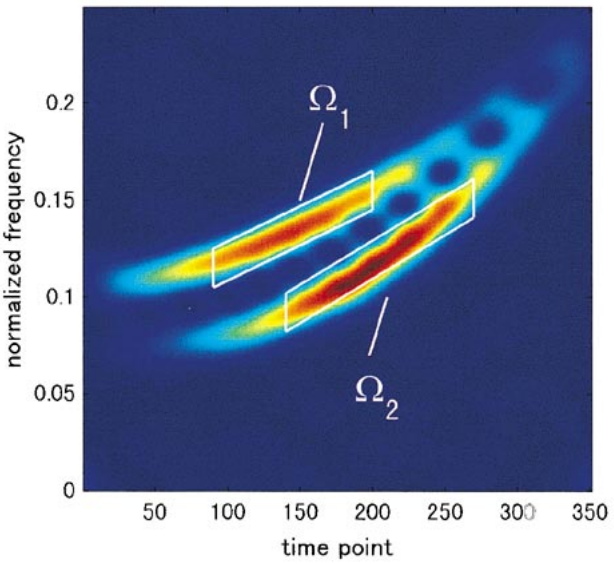

Fig. 2. Spectrogram obtained by averaging the spectrograms from all channel recordings. The two quadrangular areas denoted by Ω_1 and Ω_2, are the target regions used for the source-estimation experiments.

ented sensor lead field $\boldsymbol{L}(\boldsymbol{x})\boldsymbol{\eta}_{\rm opt}$ and the noise-level eigenvectors.

Therefore, the localizing function can be calculated in the following manner:

$$J(\boldsymbol{x}) = 1/\lambda_{\min}\left(\boldsymbol{L}^T(\boldsymbol{x})\boldsymbol{Z}_N\boldsymbol{Z}_N^H\boldsymbol{L}(\boldsymbol{x}),\, \boldsymbol{L}^T(\boldsymbol{x})\boldsymbol{L}(\boldsymbol{x})\right) \qquad (15)$$

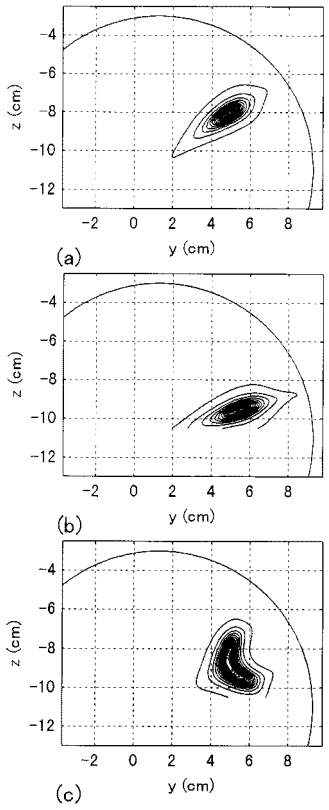

Fig. 3. Results of calculating the MUSIC localizer on the plane $x = 1$ cm. The time-frequency MUSIC algorithm was used with the target region set as: (a) Ω_1 and (b) Ω_2. (c) The conventional MUSIC algorithm was used. The contours show the relative values of the MUSIC localizer.

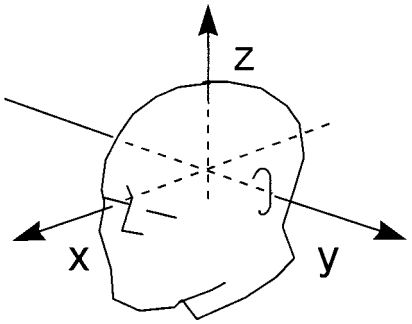

Fig. 4. The x, y, and z coordinates used to express the estimated results in Figs. 6, 8, 12, and 14. The midpoint between the left and right preauricular points is defined as the coordinate origin. The axis directed away from the origin toward the left preauricular point is defined as the $+y$ axis and that from the origin to the nasion is the $+x$ axis. The $+z$ axis is defined as the axis perpendicular to both these axes and is directed from the origin to the vertex.

where the matrix $\boldsymbol{Z}_N$ is defined as $\boldsymbol{Z}_N = [\boldsymbol{u}_{P_\Omega+1}, \ldots, \boldsymbol{u}_M]$. The only difference between the proposed and the conventional MUSIC algorithms is that the proposed algorithm uses this $\boldsymbol{Z}_N$ instead of the $\boldsymbol{E}_N$ used in (4), and that since the matrix $\boldsymbol{Z}_N$ is complex-valued, we use the Hermitian conjugate $\boldsymbol{Z}_N^H$. Equation (15) was obtained under the assumption that dipole sources do not change their orientations during the time period of interest. It can easily be shown that this localizer in (15) is effective even when this assumption does not hold and the source orientations change during the measurement [5].

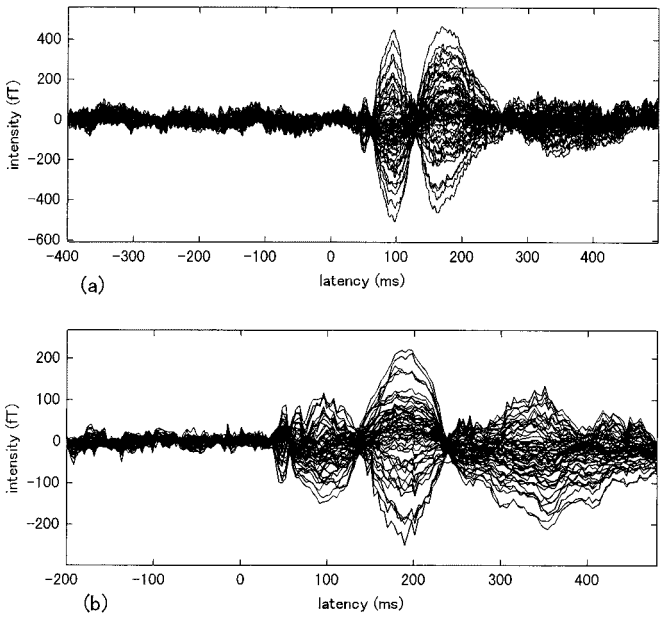

Fig. 5. MEG waveforms from two kinds of auditory measurements. (a) Regular auditory N1m measurement. (b) Auditory gamma-band measurement. The recordings from 60 sensors covering the subject's right hemisphere are overlapped.

3) Summary of the Algorithm: The procedure of implementing the time-frequency MUSIC algorithm is summarized as follows.

Step 1) The time-frequency matrix $\boldsymbol{C}_b(t, f)$ is calculated with an appropriate choice of the time-frequency representations. The mth diagonal term of this matrix is given by the auto-time-frequency distribution of the mth-channel recording, and its (m_1, m_2)th off-diagonal term is given by the cross-time-frequency distribution between the m_1th and m_2th channels.

Step 2) The matrix $\boldsymbol{\Upsilon}_b$ is obtained by averaging $\boldsymbol{C}_b(t, f)$ over the predetermined target region Ω, and the noise-level eigenvectors are obtained by applying the eigen-decomposition of $\boldsymbol{\Upsilon}_b$.

Step 3) The localizer defined by (15) is calculated throughout the source space, and each location where $J(\boldsymbol{x})$ reaches a peak is determined to be the location of one dipole source.

III. Numerical Experiments

We performed numerical experiments to test the validity of the arguments in Section II. We used the coil configuration of a 148-channel whole-head Magnes 2500 WH biomagnetic measurement system (Biomagnetic Technologies Inc., San Diego, CA). The coordinate origin was defined at the center of the coil array. The z direction was defined as the direction perpendicular to the plane of the detector coil located at this center. The x direction was defined as that from the posterior to the anterior, and the y direction was defined as that from the left to the right hemisphere. Two signal sources were assumed to exist on the same plane ($x = 1.0$ cm) with their (y, z) coordinates equal to $(5.0, -8.0)$ and $(5.5, -9.5)$.

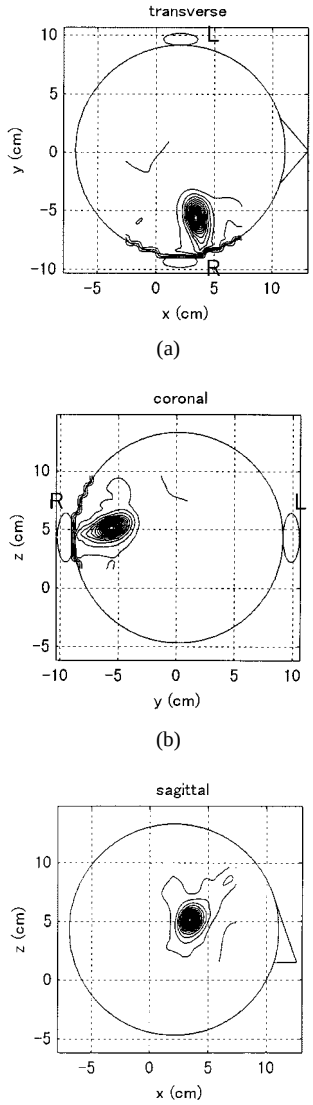

Fig. 6. Results of applying the conventional time-domain MUSIC algorithm to the data shown in Fig. 5(a). The time window ranging from 0–130 ms was used to calculate $\boldsymbol{R}_b$. The contours show the relative values of the localizer in (4); the projections of the localizer values onto the transverse, coronal, and sagittal planes are shown. The circles depicting a human head represent the projections of the sphere used to calculate the forward solution.

The simulated magnetic field was calculated at 351 time points. To generate the simulated neuromagnetic field, the ϕ components of the two sources $w_\phi^j(t)$, $(j = 1, 2)$ were amplitude- and frequency-modulated; i.e., $w_\phi^j(t) = \exp[-(t - \zeta_j)^2/(2\rho_j^2)]\cos[2\pi(\alpha_j t^2 + \beta_j t + \epsilon_j)]$. The values for $\{\zeta_j, \rho_j, \alpha_j, \beta_j, \epsilon_j\}$ were set at $\{150, 300, 1.0 \times 10^{-6}, 5.2 \times 10^{-5}, 0.105\}$ for the first source and $\{210, 280, 1.6 \times 10^{-6}, -1.3 \times 10^{-4}, 0.077\}$ for the second source where the unit of t is timepoint. Their θ components were set to zero.

Gaussian noise uncorrelated between different sensor recordings was added to make the final signal-to-noise ratio (SNR) equal to 0.85. The SNR was defined as the ratio of the Frobenius norm of the signal-magnetic-field data matrix to that of the noise matrix. The waveform of the generated magnetic field from one representative channel located approximately above

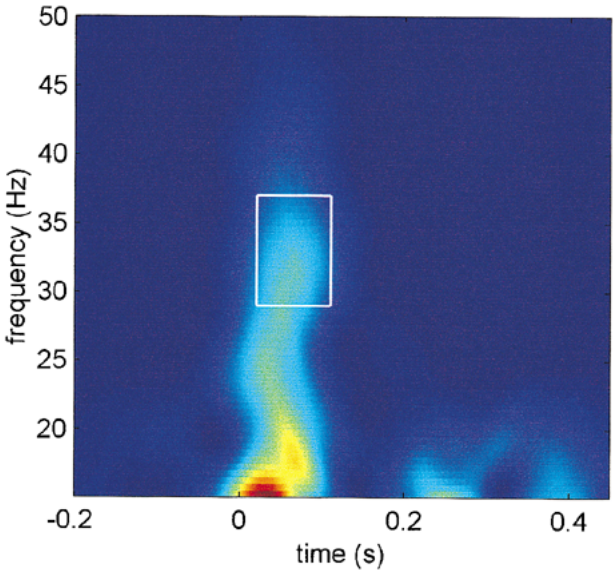

Fig. 7. Spectrogram for the frequency range above 15 Hz obtained from the MEG data in Fig. 5(b). The spectrogram was calculated using the first singular temporal vector, which was obtained by applying the singular value decomposition to the 60-channel spatio–temporal matrix of the averaged data. The windowing function was set equal to a 255-point Hanning window.

the two sources is shown in Fig. 1(a). Its power spectrum is shown in Fig. 1(b), and the power spectrum averaged across all sensor channels is shown in Fig. 1(c). The spectrograms were calculated from all channel recordings, and the results obtained by averaging all these spectrograms are shown in Fig. 2. Here, a Hanning window with a size of 77 data points was used [19]. Figs. 1 and 2 indicate that the signals from the two sources cannot be separated in either the time domain or in the frequency domain, but they are clearly separated in the time-frequency domain.

The time-frequency MUSIC algorithm was then applied by setting the target time-frequency region as the regions indicated by Ω_1 and Ω_2 in Fig. 2. The results are shown in Fig. 3. The contours in Fig. 3(a) and (b) shows the relative value of the MUSIC localizing function in (15) on the plane $x = 1$ cm, and each area where the localizing function reaches a peak is considered to be the location of one dipole source. The (y, z) coordinates of the peak locations in Fig. 3(a) and (b) are $(4.9, -8.1)$ and $(5.6, -9.5)$, respectively. These results show that the time-frequency MUSIC algorithm accurately localized these two signal sources, and these results verify the validity of our argument in Section II. The conventional time-domain MUSIC algorithm was also applied to the same computer-generated data, but the conventional algorithm was not able to resolve the two sources [Fig. 3(c)].

IV. Experiments Using MEG Data

The MEG data presented in this section was recorded by using a 148-channel whole-head biomagnetometer (Magnes 2500WH) that was installed at the Communications Research Laboratory, Tokyo, Japan. We use the head coordinates explained in Fig. 4 to express the estimated source locations.

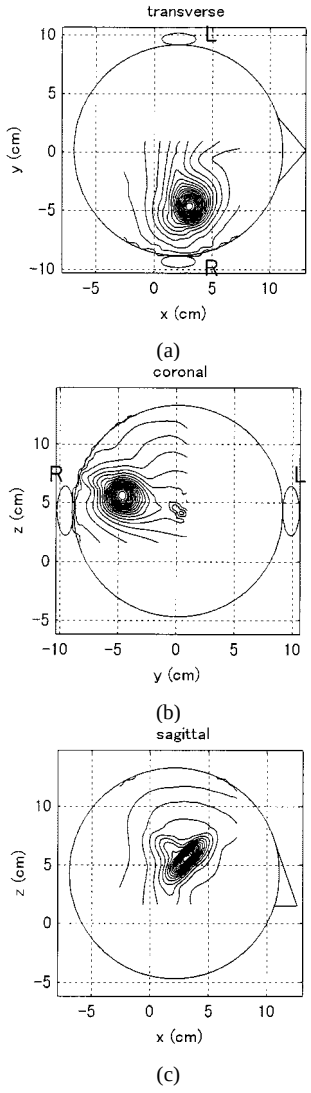

Fig. 8. The results of calculating time-frequency MUSIC localizer [(15)] with the target region set at the gamma-band region marked as the square in Fig. 7.

A. Source Localization for Auditory Gamma-Band Activity

Two kinds of auditory measurements were conducted with a healthy male volunteer (age 39, right-handed). First, we measured the regular auditory magnetic response by using a 1-kHz pure-tone stimulus applied to the subject's left ear. The sampling interval in the data acquisition was 1 kHz, the average inter-stimulus interval was 2 s, and an on-line bandpass filter ranging from 1–400 Hz was applied. A total of 100 epochs were averaged, and this averaged data is shown in Fig. 5(a). Here we selected recordings from 60 sensors covering the subject's right hemisphere and the waveforms for those recordings are overlapped in this figure. The peak for the N100m (the peak located around the latency of 100 ms) is clearly visible. Second, we measured the gamma-band auditory activity using a click sound with a duration of 1 ms. The click sound was applied to the subject's left ear; the inter-stimulus interval was 1 s and a total of 400 epochs were averaged. In this measurement, to maintain the subject's attention to the stimulus, the subject was asked to move his right index finger when he heard the tone. The waveforms from the same 60 sensors are shown in Fig. 5(b).

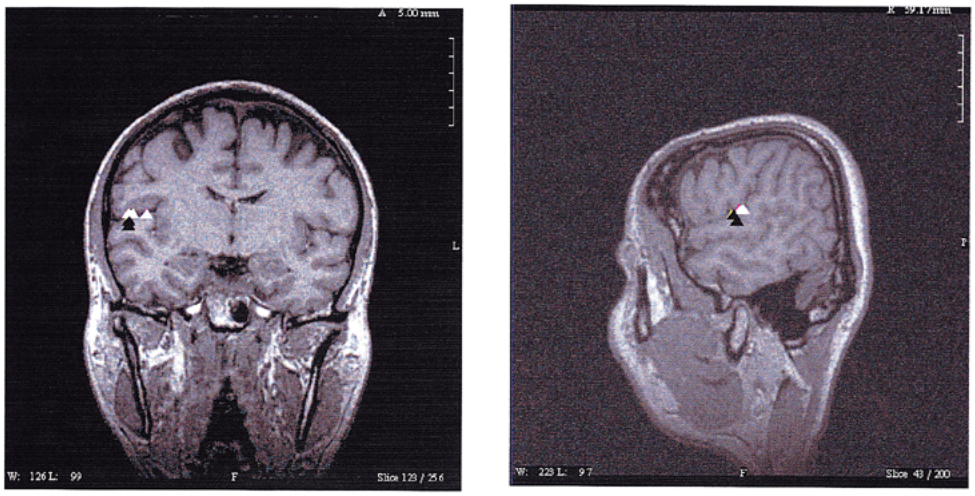

(a) (b)

Fig. 9. MRI overlay of the gamma-band source and the N1m source both obtained from three separate measurement sessions. The white and the black triangles indicate the locations of the gamma-band and the N1m sources, respectively. The coronal (left) and the sagittal (right) cross sections are shown.

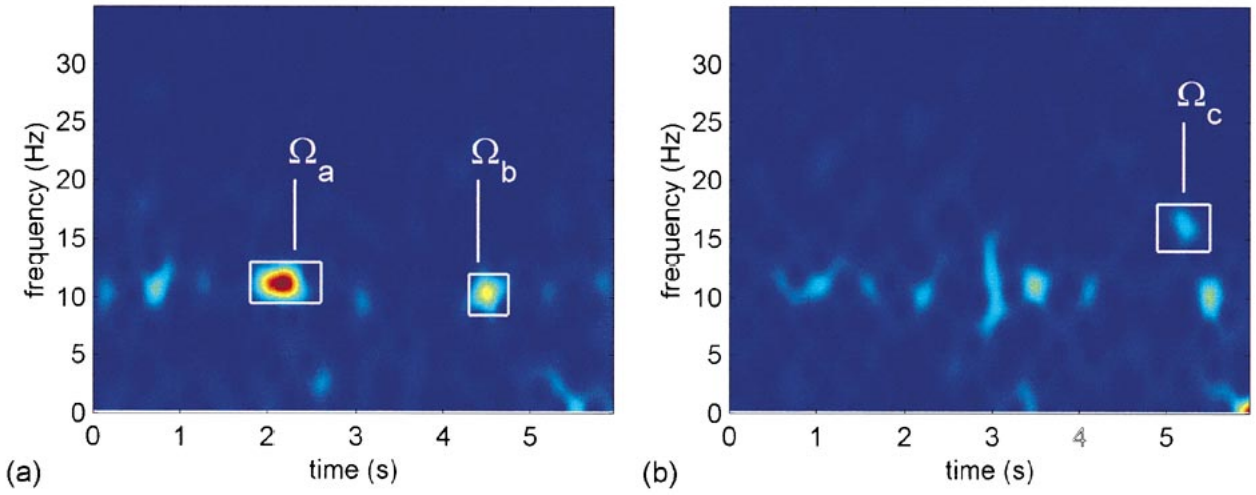

Fig. 10. Spectrograms calculated from the temporal singular vectors of the 148-channel recordings of the spontaneous MEG. (a) The first singular vector is used. (b) The second singular vector is used. The windowing function was set equal to a 127-point Hanning window. The regions denoted as Ω_a, Ω_b, and Ω_c were chosen as the target regions in the time-frequency MUSIC analysis.

We applied the conventional time-domain MUSIC algorithm to the auditory N100m shown in Fig. 5(a). The covariance matrix $\boldsymbol{R}_b$ was calculated using this averaged response with a time window ranging from 0–130 ms. The MUSIC localizer plot is shown in Fig. 6. In this figure, the MUSIC localizing function in (4) was calculated with an interval of 0.5 cm over a volume in the subject's right hemisphere, and the projections onto the transverse, the coronal, and the sagittal planes are displayed. The figure shows that the algorithm detected the source for the N100m response, which is believed to be located in the primary auditory cortex area in the right hemisphere.

To extract a representative time-course of the 60-channel recordings shown in Fig. 5(b), we applied the singular value decomposition to the spatio–temporal data matrix of these averaged recordings. The spectrogram was then calculated using the first temporal singular vector, which corresponds to the largest singular value. The windowing function was set equal to a 255-point Hanning window. The results are shown in Fig. 7. The stimulus-locked gamma-band activity is clearly observed in the latency range from 0–0.1 s. The MUSIC localizer plot obtained using (15) is shown in Fig. 8. Here, the procedure described in Section II-C-3 was applied to the averaged data in Fig. 5(b). That is, the averaged data was used as $\boldsymbol{b}(t)$ in (5). The square in Fig. 7 indicates the target region; i.e., only the gamma-band portion within this square was used to obtain the plot in Fig. 8. In this figure, the time-frequency MUSIC method clearly detected a single localized source for the auditory gamma-band activity in the right temporal area.

With this subject, we repeated the same measurements three times; each measurement session was separated by approximately one week. The three sets of localized results for the gamma-band activity were overlayed onto the subject's magnetic resonance image (MRI). The results are shown in Fig. 9. The three locations of the gamma-band source were all medial to the N100m source but differed somewhat: One was located nearly 1 cm medial to the N100m source, but the other two were close to the N100m source.

B. Source Localization for Spontaneous MEG

The subject was a healthy male volunteer (age 27, right-handed) who was asked to lie down quietly with his eyes closed during the measurements. The spontaneous MEG was recorded continuously for a total of six seconds with a sampling frequency of 677~Hz. An on-line bandpass filter ranging from 1~Hz to 200~Hz was applied. Singular-value decomposition of the 148-channel spatio-temporal data matrix was performed, and spectrograms were obtained from the first and the second temporal singular vectors. The windowing function was set equal to a 127-point Hanning window. The resultant spectrograms are shown in Fig. 10. A part of the 148-channel recordings of the spontaneous MEG is shown in Fig. 11. A couple of the alpha spindles can be observed in this figure.

Two distinct alpha bursts are clearly observed in Fig. 10(a), which was obtained from the first singular vector. The regions including these components are denoted as Ω_a and Ω_b as shown in Fig. 10(a). Then, the time-frequency MUSIC algorithm was applied with the target region set at Ω_a and Ω_b. The MUSIC localizer plots are shown in Fig. 12(a) and (b). Fairly localized sources were detected and the locations of the sources from Ω_a and Ω_b were found in the occipital region. The region marked by Ω_c in Fig. 10(b) was also analyzed by the time-frequency MUSIC algorithm. The resultant MUSIC localizer plot is shown in Fig. 12(c) A single source is clearly detected in the left temporal area.

The peak locations in Fig. 12(a)– (c) were overlayed onto the subject's MRI; the results for sagittal cross sections are shown in Fig. 13. The two sources for the alpha bursts in Ω_a and Ω_b are, respectively, localized near the parieto-occipital sulcus and in the occipital visual area [Fig. 13(a) and (b)]. Several previous investigations reported that the source for the alpha rhythm was localized near the parieto-occipital sulcus and near the calcarine sulcus in the visual area [10]–[12]. It was also reported that each alpha burst (spindle) has its own location [20], [21]. Our results here are in good agreement with the results from these previous investigations. Fig. 13(c) shows that the source for a component in Ω_c was localized in the motor area, and this indicates that this component is a part of the mu-rhythm [10], [12]. These results show that the time-frequency MUSIC algorithm is so sensitive that it was able to detect the mu-rhythm source from the alpha-rhythm-dominant spontaneous MEG.

V. Discussion

In the results presented in Section IV-A, the three locations of the gamma-band source were all medial to the N100m source but differed somewhat. A previous investigation [8], [9] reported that the source of the gamma-band activity was localized slightly medial and anterior to the N100m source. Our results are in fairly good agreement with these previous results. Several factors could have caused the fluctuation in the estimated source locations of the auditory gamma-band activity. Such factors include errors in registering the head coordinates to the MRI pixel coordinates, the subject's head motion during the measurement, and the noise contained in the target time-frequency region. Even fluctuations in the subject's internal conditions, such as his attention to the stimulus [9] or his general vigilance level, may have caused fluctuation of the estimated source locations. Further investigation using multiple subjects is needed to draw clearer conclusions about the location of the source of the gamma-band activity.

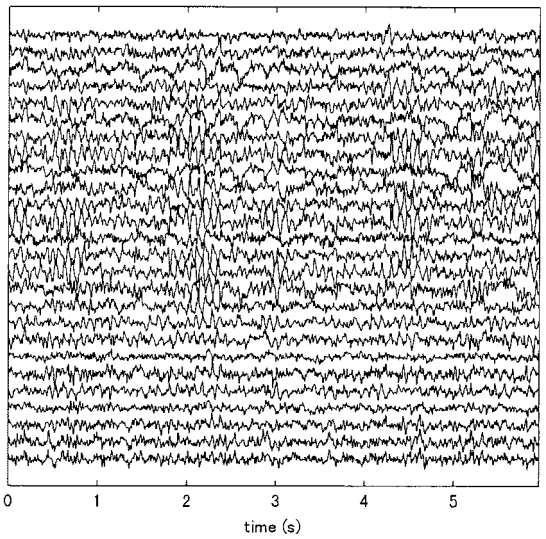

Fig. 11. The measured spontaneous MEG. Twenty-six representative channel recordings were selected. (The selection was made with no particular preference, and these 26 channel sensors are fairly uniformly located on a head surface.) This spontaneous MEG was measured for 6 s with a subject lying down quietly with his eyes closed.

We also applied the conventional time-domain MUSIC algorithm to the spontaneous MEG data in Section IV-B for comparison. The results are shown in Fig. 14. Here, data from the whole 6 s was used to obtain $\boldsymbol{R}_b$. The results indicate that the conventional MUSIC algorithm can resolve none of the sources detected by the time-frequency MUSIC algorithm, and the conventional MUSIC algorithm only detected a large activated area in the occipital region. This comparison demonstrates the effectiveness of the proposed time-frequency MUSIC algorithm for selectively localizing sources having different time-frequency signatures.

In Section II, the time-frequency MUSIC algorithm was derived from the matrix equation [(12)] with the assumption that there are no perfectly correlated sources. The MUSIC algorithm has a well-known problem in that it tends to mis-localize sources when they are highly correlated. It is, therefore, worth noting that the developed method can be modified to incorporate non-MUSIC-type multidipole estimation. It can be shown that the optimum estimates of the source locations can be obtained by directly minimizing the least-squares-error cost function given by

$$\mathcal{F} = \mathbf{\Pi}\boldsymbol{\Upsilon}_b\mathbf{\Pi}^T \tag{16}$$

where $\mathbf{\Pi}$ is the projection operator defined as

$$\mathbf{\Pi} = \boldsymbol{I} - \left(\hat{\boldsymbol{L}}_c\hat{\mathbf{\Psi}}\right)\left[\left(\hat{\boldsymbol{L}}_c\hat{\mathbf{\Psi}}\right)^T\left(\hat{\boldsymbol{L}}_c\hat{\mathbf{\Psi}}\right)\right]^{-1}\left(\hat{\boldsymbol{L}}_c\hat{\mathbf{\Psi}}\right)^T \tag{17}$$

and $\hat{\boldsymbol{L}}_c$ and $\hat{\mathbf{\Psi}}$ are the estimated values of $\boldsymbol{L}_c$ and $\mathbf{\Psi}$. This minimization can be done using conventional nonlinear optimiza-

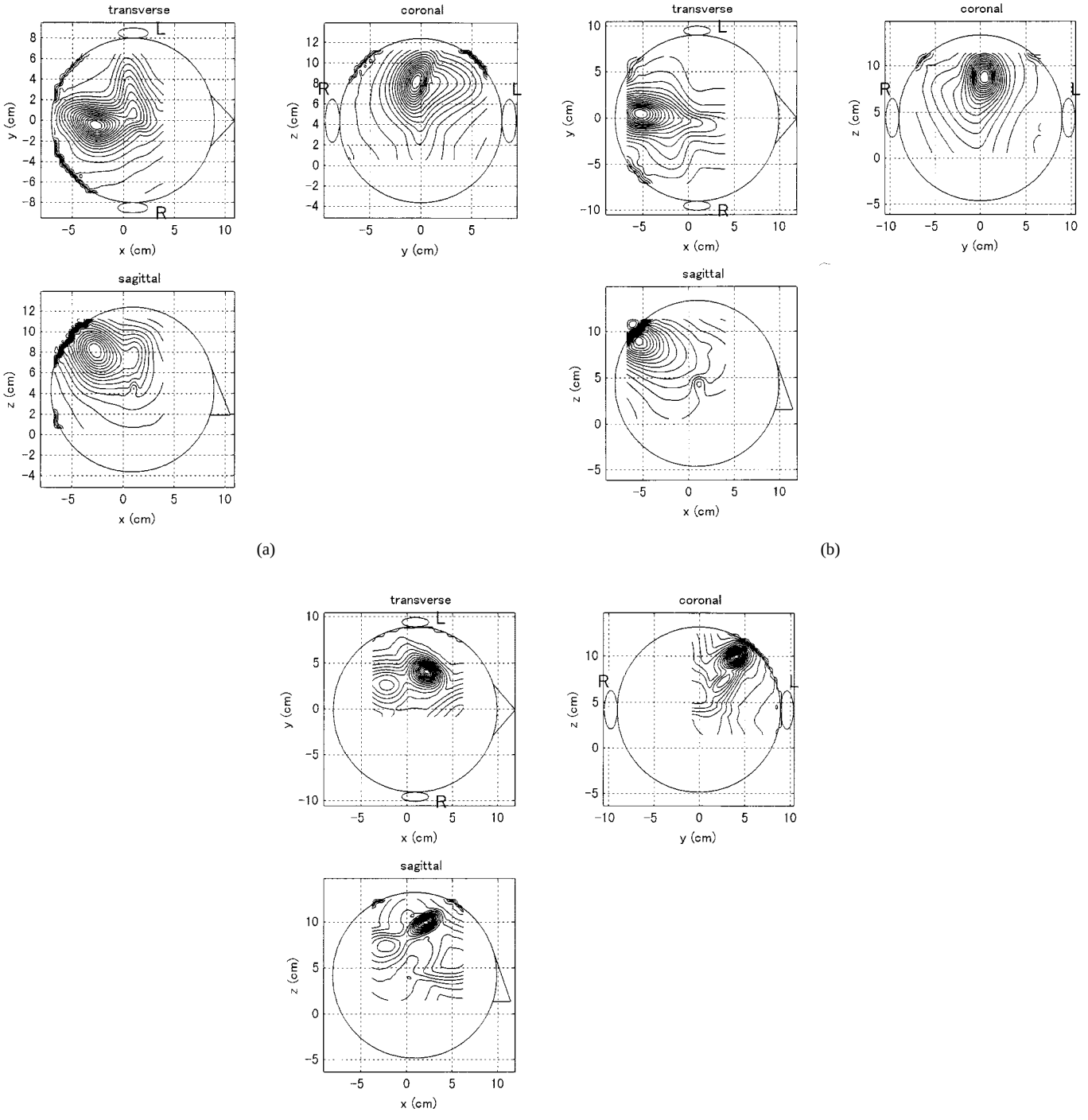

Fig. 12. The results of applying the time-frequency MUSIC algorithm to the spontaneous MEG data. The target region was set at (a) Ω_a, (b) Ω_b, and (c) Ω_c.

tion methods [19]. Thus, if it is suspected that correlated multiple sources exist in the time-frequency ROI, we can apply this direct minimization procedure although we need information about the number of sources and a good initial guess concerning the source locations.

The most computationally intensive part of implementing the time-frequency MUSIC algorithm is the calculation of $\boldsymbol{C}_b(t, f)$, which contains M^2 times calculations of the cross- or auto-time-frequency distribution of channel recordings. In Section IV, we used the STFT because of its computational efficiency. For the case presented in Section IV-A, it took approximately one hour[1] to calculate $\boldsymbol{\Upsilon}_b$, but we estimated

[1]This calculation was done by using Pentium III (450 MHz)-based PC with MATLAB (Mathworks, Natick, MA).

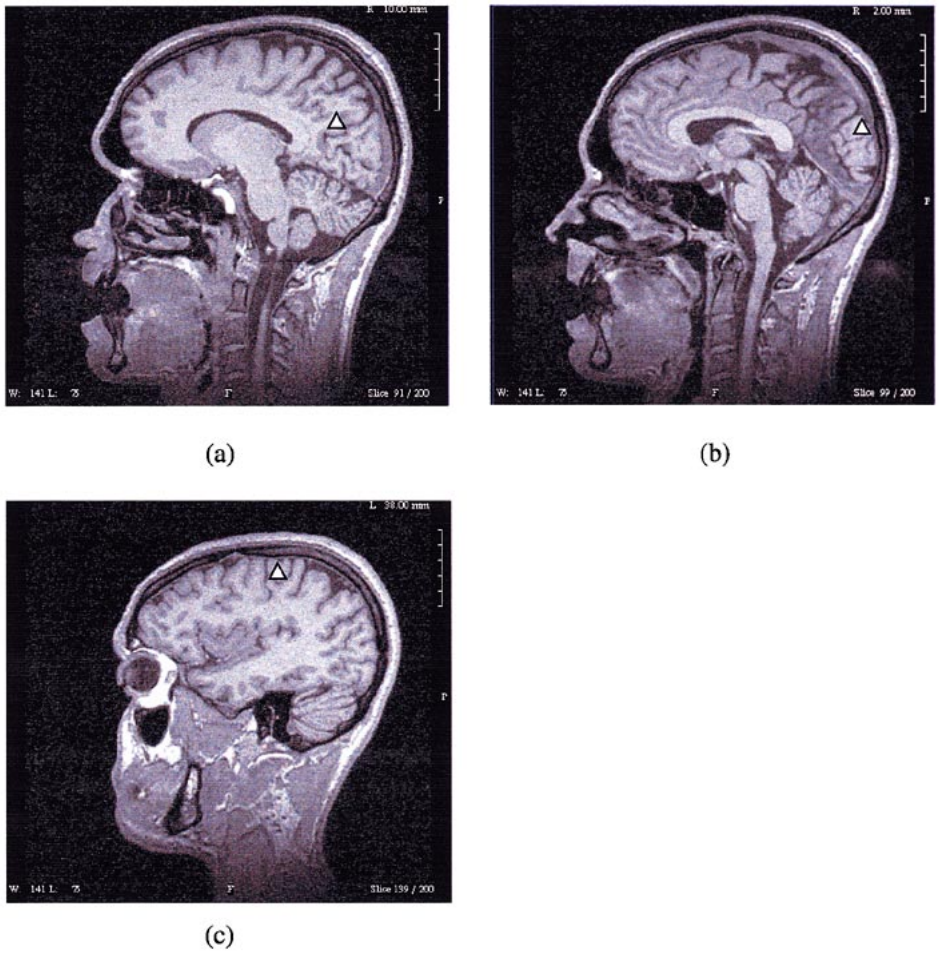

Fig. 13. MRI overlay of the peak locations in Fig. 12. The results in (a), (b), and (c), respectively, show the peak locations obtained in Fig. 12(a)–(c).

that it would have taken 3–4 h to calculate this matrix if we had used the smoothed pseudo Wigner distribution, which is a typical Cohen-class quadratic representation. The current computer routine, however, is not optimized to obtain the highest performance in the computational speed, and it is possible to attain a considerable speedup, for example, by programing it using the C code. For analyzing MEG data such as those presented in Section IV, any time-frequency representations could be used with the time-frequency MUSIC algorithm because high time-frequency resolution is not needed to analyze such MEG data. However, when analyzing other kinds of MEG data, such as some types of sleep spindles or epileptic spikes, it may be necessary to use more sophisticated time-frequency representations, since analyzing such data may require higher time-frequency resolution. Computer routine that calculates $\boldsymbol{C}_b(t,\ f)$ with a resonable computational speed should be developed in such cases.

A time-frequency representation of multichannel MEG recordings provides space, time, and frequency information, and many time-frequency maps whose number equals the number of sensor channels are obtained. Such information may be excessive for extracting the time-frequency characteristics of the signal of interest, and we need to obtain fewer time-frequency maps that appropriately represent the whole time-frequency properties of the multichannel data. To extract such representative time-frequency maps, we applied singular-value decomposition to the measured spatio–temporal data matrix in Section IV, and calculated the time-frequency maps of the temporal singular vectors corresponding to significantly large singular values. Other method can also be used, for example, one that calculates the time-frequency distribution averaged over the channels [this is equivalent to calculating the trace of the matrix $\boldsymbol{C}_b(t,\ f)$]. A simpler method such as this may suffice in some cases such as our numerical experiment in Section III.

In summary, we have developed a method that incorporates the time-frequency characteristics of neural sources into magnetoencephalographic (MEG) source estimation. The method, which we refer to as the time-frequency MUSIC algorithm, allows the locations of neural sources to be estimated from any time-frequency ROI. The algorithm was applied to two types of nonstationary MEG data: auditory gamma-band activity data and spontaneous MEG data. The effectiveness of the time-frequency MUSIC algorithm was assessed by comparing the results of these applications with the results from previous investigations on the same types of nonstationary MEG data. As a next step, we plan to apply the proposed time-frequency MUSIC algorithm to MEG data whose origin is difficult to analyze with existing methods. Possible candidates include some types of sleep spindles, epileptic spikes, and spontaneous waves with pathologic origins. The results of these investigations will be reported in the near future.

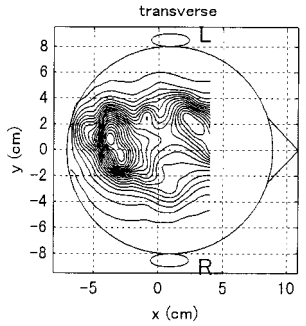

(a)

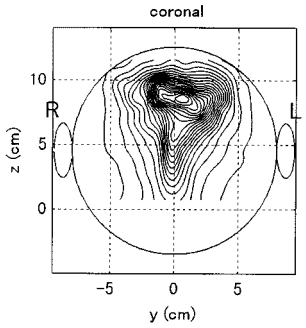

(b)

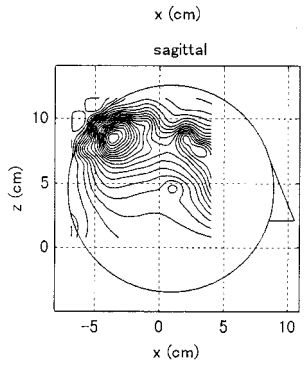

(c)

Fig. 14. The results of applying the conventional time-domain MUSIC algorithm (4) to the spontaneous MEG data. Data from the whole 6 s was used to calculate the covariance matrix $\boldsymbol{R}_t$.

ACKNOWLEDGMENT

The authors would like to thank Dr. R. Takino for his help in performing the MEG measurements. A part of the computer simulation reported in this paper used the Time-Frequency Toolbox provided by France's CNRS (Centre National de la Recherche Scientifique).

REFERENCES

[1] M. Hämäläinen, R. Hari, R. J. IImoniemi, J. Knuutila, and O. V. Lounasmaa, "Magnetoencephalography–theory, instrumentation, and applications to noninvasive studies of the working human brain," *Rev. Mod. Phys.*, vol. 65, pp. 413–497, 1993.

[2] C. Tallon-Baudry, O. Bertr, C. Delpuech, and J. Pernier, "Stimulus specificity of phase-locked and nonphase-locked 40-Hz visual responses in human," *J. Neurosci.*, vol. 16, pp. 4240–4249, 1996.

[3] C. Tallon-Baudry, O. Bertrand, C. Delpuech, and J. Pernier, "Oscillatory γ-band (30–70 Hz) activity induced by a visual search task in humans," *J. Neurosci.*, vol. 17, pp. 722–733, 1997.

[4] E. Rodriguez, N. George, J. P. Lachaux, J. Martinerie, B. Renault, and F. J. Varela, "Perception's shadow: Long-distance synchronization of human brain activity," *Nature*, vol. 397, pp. 430–433, 1999.

[5] K. Sekihara, S. Nagarajan, D. Poeppel, and Y. Miyashita, "Time-frequency MEG-MUSIC algorithm," *IEEE Trans. Med. Imag.*, vol. 18, pp. 92–97, 1999.

[6] M. Sun, S. Qian, X. Yan, S. B. Baumann, X.-G. Xia, R. E. Dahl, N. D. Ryan, and R. J. Sclabassi, "Localizing functional activity in the brain through time-frequency analysis and synthesis of the EEG," *Proc. IEEE*, vol. 84, pp. 1302–1311, 1996.

[7] M. Amin and A. Belouchrai, "Time-frequency MUSIC," in *Proc. SPIE Symp. Radar Processing, Technology, and Applications*, San Diego, CA, July 1998.

[8] C. Pantev, T. Elbert, S. Makeig, S. Hampson, C. Eulitz, and M. Hoke, "Relationship of transient and steady-state auditory evoked fields," *Electroenceph. Clin. Neurophysiol.*, vol. 88, pp. 389–396, 1993.

[9] C. Pantev and T. Elbert *et al.*, "The transient auditory evoked gamma-band field," in *Oscillatory Event-Related Brain Dynamics*, C. Pntev *et al.*, Eds. New York: Plenum, 1994, pp. 219–230.

[10] R. Hari and R. Salmelin, "Human cortical oscillations: A neuromagnetic view through the skull," *Trends Neurosci.*, vol. 20, pp. 44–49, 1997.

[11] C. Tesche and M. Kajola, "A comparison of the localization of spontaneous neuromagnetic activity in the frequency and time domains," *Electroenceph. Clin. Neurophysiol.*, vol. 87, pp. 408–416, 1993.

[12] R. Salmelin and R. Hari, "Caracterization of spontaneous MEG rhythms in healthy adults," *Electroenceph. Clin. Neurophysiol.*, vol. 91, pp. 237–248, 1994.

[13] J. Sarvas, "Basic mathematical and electromagnetic concepts of the biomagnetic inverse problem," *Phys. Med. Biol.*, vol. 32, pp. 11–22, 1987.

[14] R. O. Schmidt, "A signal subspace approach to multiple emitter location and spectral estimation," Ph.D. dissertation, Stanford University, Stanford, CA, 1981.

[15] J. C. Mosher, P. S. Lewis, and R. M. Leahy, "Multiple dipole modeling and localization from spatio–temporal MEG data," *IEEE Trans. Biomed. Eng.*, vol. 39, pp. 541–557, 1992.

[16] F. Hlawatsch and G. F. Boudreaux-bartels, "Linear and quadratic time-frequency signal representations," *IEEE Signal Processing Magazine*, vol. 9, pp. 21–67, 1992.

[17] L. Cohen, *Time-Frequency Analysis: Theory and Applications*. Englewood Cliffs, NJ: Prentice-Hall, 1994.

[18] L. Cohen, "Time-frequency distributions—A review," *Proc. IEEE*, vol. 77, pp. 941–981, 1989.

[19] W. H. Press, S. A. Teukolsky, W. T. Vetterling, and B. P. Flannery, *Numerical Recipes in Fotran: The Art of Scientific Computing*, 2nd ed. New York: Cambridge Univ. Press, 1992.

[20] S. J. Williamson, J.-Z. Wang, and R. J. Ilmoniemi *et al.*, "Method for localizing sources of human alpha activity," in *Advances in Biomagnetism*, S. J. Williamson *et al.*, Eds. New York: Plenum Press, 1989, pp. 257–260.

[21] R. M. Chapman *et al.*, "EEG/MEG and alpha activity: Current status of biomagnetic research," in *Biomagnetism Clinical Aspects*, M. Hoke *et al.*, Eds. Ansterdam, The Netherlands: Elsevier Science, 1992, pp. 25–31.

Kensuke Sekihara (M'88) received the M.S. and Ph.D. degrees from Tokyo Institute of Technology, Tokyo, Japan, in 1976 and 1987, respectively.

Since 1976, he has worked with Central Research Laboratory, Hitachi, Ltd., Tokyo, Japan. He was a Visiting Research Scientist at Stanford University, Stanford, CA from 1985 to 1986, and at Basic Development, Siemens Medical Engineering, Erlangen, Germany, from 1991 to 1992. He is currently working with "Mind Articulation" research project sponsored by Massachusetts Institute of Technology and Japan Science and Technology Corporation. His research interests include the biomagnetic inverse problems, and statistical estimation theory, especially its application to noninvasive measurements of brain functions.

Dr. Sekihara is a member of IEEE Medicine and Biology Society, IEEE Signal Processing Society, and International Society of Magnetic Resonance in Medicine.

Srikantan S. Nagarajan received the B.S. degree in electrical engineering from the University of Madras, Madras, India, and the M.S. and Ph.D. degrees from the Department of Biomedical Engineering, Case Western Reserve University, Cleveland, OH, in 1993 and 1995, respectively.

From 1995–1998, he was a Postdoctoral Fellow in the Keck Center for Integrative Neuroscience at the University of California, San Francisco (UCSF). Since 1999, he has been a full-time Research Scientist at Scientific Learning Corporation, Berkeley, CA, and is an Adjunct Assistant Professor in the Department of Otolaryngology at UCSF. In January 2000, he will start as an Assistant Professor in the Department of Bioengineering at the University of Utah, Salt Lake City. His research interests in neural engineering include bio-electromagnetism, systems and computational neuroscience and statistical signal processing.

David Poeppel received the B.S. and Ph.D. degrees in cognitive neuroscience from Massachusetts Institute of Technology, Cambridge, in 1990 and 1995, respectively.

He is currently an Adjunct Assistant Professor in the Department of Radiology, University of California, San Francisco, and an Assistant Professor in the Departments of Linguistics and Zoology at the University of Maryland, College Park. His research uses the functional neuroimaging methods, magnetoencephalography (MEG), and functional magnetic resonance imaging (fMRI) to investigate the neural basis of speech and language processing.

Satoru Miyauchi received the B.S. degree in psychology from Waseda University, Tokyo, Japan, in 1977, and the Ph.D. degree in medical sciences at Toho University, Tokyo, Japan, in 1990.

He is currently a Section Chief of Auditory and Visual Informatics Section, Kansai Advanced Research Center, Communications Research Laboratory, Hyogo, Japan. His research uses functional magnetic resonance imaging (fMRI) and magnetoencephalography (MEG) to investigate the neural basis of visual attention and visual imagery.

Norio Fujimaki received the B.S., M.S., and Ph.D. degrees in electronics engineering from the University of Tokyo, Tokyo, Japan, in 1975, 1977, and 1980, respectively.

He worked in Fujitsu Laboratories Ltd., Atsugi, Japan, from 1980 to 1999. In 1999, he joined Communications Research Laboratory. His research interests are superconducting devices and brain-function measurements using electroencephalograpy, magentoencephalography, and functional magnetic resonance imaging.

Hideaki Koizumi was born in Tokyo, Japan, in 1946. He graduated from the Department of Pure and Applied Sciences at the University of Tokyo, Tokyo, Japan in 1971. He received the doctoral degree in physics from the University of Tokyo in 1976 for his dissertation creating polarized Zeeman-effect atomic absorption spectrometry.

He joined Hitachi, Ltd., Tokyo, Japan. After receiving the Ph.D. degree, he remained as Visiting Faculty at the Lawrence Berkeley Laboratory, University of California, Livermore, from 1978 to 1979. Upon returning to Japan, he led MRI development projects. He now leads projects on environmental measurement and analysis and noninvasive higher-order brain function analysis. He is a Chief Research Scientist at the Central Research Laboratory, Hitachi, Ltd. and a Professor of the Research Institute for Electronic Science, Hokkaido University, Sapporo, Japan.

Dr. Koizumi received many awards such as the Ohkochi Memorial Prize, the Prize of Science and Technology Minister, and IR-100. He is also a member of the board of directors of the Chemical Society of Japan.

Yasushi Miyashita received the Ph.D. degree in physiology from the University of Tokyo, Tokyo, Japan, in 1979.

He is currently Professor and Chairman of the Physiology Department at the University of Tokyo School of Medicine, Tokyo, Japan. His research interests include neural basis of cognition in primates, functional imaging, and image processing with MRI, MEG, and optical devices.